Supporting Information for "Evolution of Denmark Strait Overflow Cyclones and Their Relationship to Overflow Surges"

M. Almansi[1] *, T. W. N. Haine[1], R. Gelderloos[1], and R. S. Pickart[2]

[1]Department of Earth and Planetary Sciences, The Johns Hopkins University

[2]Woods Hole Oceanographic Institution

Contents of this file

1. Text S1
2. Figure S1

Introduction This supplementary information contains additional details of the automatic vortex detection scheme that we designed to isolate DSO features. We include a

---

Corresponding author: M. Almansi, Department of Earth and Planetary Sciences, The Johns Hopkins University, 301 Olin Hall - 3400 N. Charles Street, Baltimore, MD 21218, USA. (mattia.almansi@jhu.edu)

* 301 Olin Hall - 3400 N. Charles Street,

Baltimore, MD 21218, USA

step-by-step description of the algorithm (Text S1), and we show the unfiltered locations of the vortices detected (Figure S1).

Text S1. We designed an automatic vortex detection scheme based on the Okubo-Weiss parameter (OW; Okubo, 1970; Weiss, 1991) to isolate DSO mesoscale features:

$$\mathrm{OW} = S_n^2 + S_s^2 - \zeta^2. \tag{1}$$

S_n, S_s, and ζ are, respectively, the normal component of the strain, the shear component of the strain, and the relative vorticity of the horizontal velocity field:

$$\begin{aligned} S_s &= \frac{\partial v}{\partial x} + \frac{\partial u}{\partial y}, \\ S_n &= \frac{\partial u}{\partial x} - \frac{\partial v}{\partial y}, \\ \zeta &= \frac{\partial v}{\partial x} - \frac{\partial u}{\partial y}. \end{aligned} \tag{2}$$

Several methods have been used in previous studies to detect mesoscale features (Lian et al., 2019). Most of them are based on sea surface fields. The following arguments motivated our choice to use the OW parameter: (i) Strain and relative vorticity can be computed from the velocity field in the middle of the water column (Equation 1), where the signal of DSO cyclones is strongest (von Appen et al., 2014); (ii) DSO cyclones are characterized by high relative vorticity, and the Okubo-Weiss scheme allows one to discern vorticity-dominated features ($\mathrm{OW} < 0$) from the background state; (iii) The typical magnitude of the OW parameter does not vary significantly in the water column, and we can define a depth-independent threshold to detect DSO cyclones along terrain-following levels.

Dense overflows are known to vary in their proximity to the seafloor (Shapiro et al., 2003). Therefore, the detection algorithm operates on three terrain-following levels (σ-

levels). We extracted the σ-levels using a nearest-neighbor vertical interpolation. Defining H as the seafloor depth, the uppermost level is located at a depth of $H/2$ (where measurements show the strongest signal of DSO cyclones; von Appen et al., 2014), the deepest level is located at $3H/4$ (in proximity to the DSO interface), and the mid-level is halfway between the top and bottom levels. Unless otherwise specified, the results shown and discussed hereafter refer to the mid-level ($5H/8$).

Our detection algorithm includes several filters to overcome the sensitivity to noise of OW (Souza et al., 2011). In line with most of the Okubo-Weiss schemes designed to detect ocean eddies (e.g., Isern-Fontanet et al., 2006), the first step of the algorithm locates vorticity dominated regions with OW $< -0.2\sigma_{OW}$, where σ_{OW} is the spatial standard deviation of OW calculated at each snapshot and σ-level. For each of the terrain-following levels, closed contours bounding these regions have been deemed as vortices and fit to ellipses. A size filter excludes features with semi-minor axis smaller than 7.8 km, which is the mean radius of DSO cyclones measured by von Appen et al. (2014) at the Spill Jet section. Furthermore, ellipses with area larger than $4\pi^2 L_D^2$, which tend not to be mesoscale features, are excluded (Klocker & Abernathey, 2014; Martínez-Moreno et al., 2019), where $L_D = 7.7$ km is the nearest first-baroclinic Rossby radius of deformation computed by Chelton, deSzoeke, Schlax, El Naggar, and Siwertz (1998) (note that the observational radius is consistent with the theoretical radius). More permissive size filters mainly affect the number of vortices detected near the Spill Jet section, where the vortices are smaller, but do not impact the results discussed in this study. Furthermore, because of the model horizontal resolution, the mean properties of vortices with axes lower than the

threshold chosen might be significantly impacted by noise. Finally, in order to exclude potential DSO cyclones without vertical coherence, the algorithm only retains features with a signal in the entire lower half of the water column (overlapping ellipses in all σ-levels).

Figure S1 shows the location of the centers of the mesoscale vortices detected. The majority of the cyclones ($\overline{f^{-1}\zeta} > 0$; overlined quantities correspond to spatial averages in the regions occupied by the vortices and f is the vertical component of the Coriolis parameter) are located in proximity to the DSO path and move southward along the continental slope (Figure S1a). By contrast, most of the anticyclones ($\overline{f^{-1}\zeta} < 0$) are located over Dohrn Bank and on the western side of the Denmark Strait trough (Figure S1b). These anticyclones move southwestward following the edge of the East Greenland shelf. We applied a set of additional filters to exclude features unrelated to the DSO. Only mesoscale features covering regions with $\bar{H}$ greater than 450 m are retained. This threshold excludes the vortices on the East Greenland shelf that do not interact with the DSO. Furthermore, we applied a distance threshold to exclude the cyclones far from the DSO path. Downstream of station #04, where the DSO moves along the continental slope, we excluded vortices with centers located farther than 20 km from the DSO path. Specifically, this filter excludes the cyclones in the Kangerdlugssuaq Trough and the anticyclones on the edge of the East Greenland shelf. Upstream of station #05, where the isobaths are far apart, we applied the same spatial filter exclusively to the vortices detected on the southeast side of the DSO path. This filter retains the anticyclones that cross Denmark Strait on the

western side of the trough, which are related to a fraction of DSO cyclones observed at the Spill Jet section (von Appen et al., 2017).

References

Chelton, D. B., deSzoeke, R. A., Schlax, M. G., El Naggar, K., & Siwertz, N. (1998). Geographical variability of the first baroclinic rossby radius of deformation. *Journal of Physical Oceanography*, *28*(3), 433-460. Retrieved from https://doi.org/10.1175/1520-0485(1998)028<0433:GVOTFB>2.0.CO;2 doi: 10.1175/1520-0485(1998)028⟨0433:GVOTFB⟩2.0.CO;2

Isern-Fontanet, J., García-Ladona, E., & Font, J. (2006). Vortices of the mediterranean sea: An altimetric perspective. *Journal of Physical Oceanography*, *36*(1), 87-103. Retrieved from https://doi.org/10.1175/JPO2826.1 doi: 10.1175/JPO2826.1

Klocker, A., & Abernathey, R. (2014). Global patterns of mesoscale eddy properties and diffusivities. *Journal of Physical Oceanography*, *44*(3), 1030-1046. Retrieved from https://doi.org/10.1175/JPO-D-13-0159.1 doi: 10.1175/JPO-D-13-0159.1

Lian, Z., Sun, B., Wei, Z., Wang, Y., & Wang, X. (2019). Comparison of eight detection algorithms for the quantification and characterization of mesoscale eddies in the south china sea. *Journal of Atmospheric and Oceanic Technology*, *36*(7), 1361-1380. Retrieved from https://doi.org/10.1175/JTECH-D-18-0201.1 doi: 10.1175/JTECH-D-18-0201.1

Martínez-Moreno, J., Hogg, A. M., Kiss, A. E., Constantinou, N. C., & Morrison, A. K. (2019). Kinetic energy of eddy-like features from sea surface altimetry. *Journal of Advances in Modeling Earth Systems*, *0*(ja). Retrieved from https://

agupubs.onlinelibrary.wiley.com/doi/abs/10.1029/2019MS001769 doi: 10.1029/2019MS001769

Okubo, A. (1970). Horizontal dispersion of floatable particles in the vicinity of velocity singularities such as convergences. *Deep Sea Research and Oceanographic Abstracts*, *17*(3), 445 - 454. Retrieved from http://www.sciencedirect.com/science/article/pii/0011747170900598 doi: https://doi.org/10.1016/0011-7471(70)90059-8

Shapiro, G. I., Huthnance, J. M., & Ivanov, V. V. (2003). Dense water cascading off the continental shelf. *Journal of Geophysical Research: Oceans*, *108*(C12). Retrieved from https://agupubs.onlinelibrary.wiley.com/doi/abs/10.1029/2002JC001610 doi: 10.1029/2002JC001610

Souza, J. M. A. C., de Boyer Montégut, C., & Le Traon, P. Y. (2011). Comparison between three implementations of automatic identification algorithms for the quantification and characterization of mesoscale eddies in the south atlantic ocean. *Ocean Science*, *7*(3), 317–334. Retrieved from https://www.ocean-sci.net/7/317/2011/ doi: 10.5194/os-7-317-2011

von Appen, W.-J., Mastropole, D., Pickart, R. S., Valdimarsson, H., Jónsson, S., & Girton, J. B. (2017). On the nature of the mesoscale variability in denmark strait. *Journal of Physical Oceanography*, *47*(3), 567-582. Retrieved from https://doi.org/10.1175/JPO-D-16-0127.1 doi: 10.1175/JPO-D-16-0127.1

von Appen, W.-J., Pickart, R. S., Brink, K. H., & Haine, T. W. (2014). Water column structure and statistics of denmark strait overflow water cyclones. *Deep Sea Research*

Part I: Oceanographic Research Papers, *84*, 110 - 126. Retrieved from http://www.sciencedirect.com/science/article/pii/S0967063713002197 doi: https://doi.org/10.1016/j.dsr.2013.10.007

Weiss, J. (1991). The dynamics of enstrophy transfer in two-dimensional hydrodynamics. *Physica D: Nonlinear Phenomena*, *48*(2), 273 - 294. Retrieved from http://www.sciencedirect.com/science/article/pii/016727899190088Q doi: https://doi.org/10.1016/0167-2789(91)90088-Q

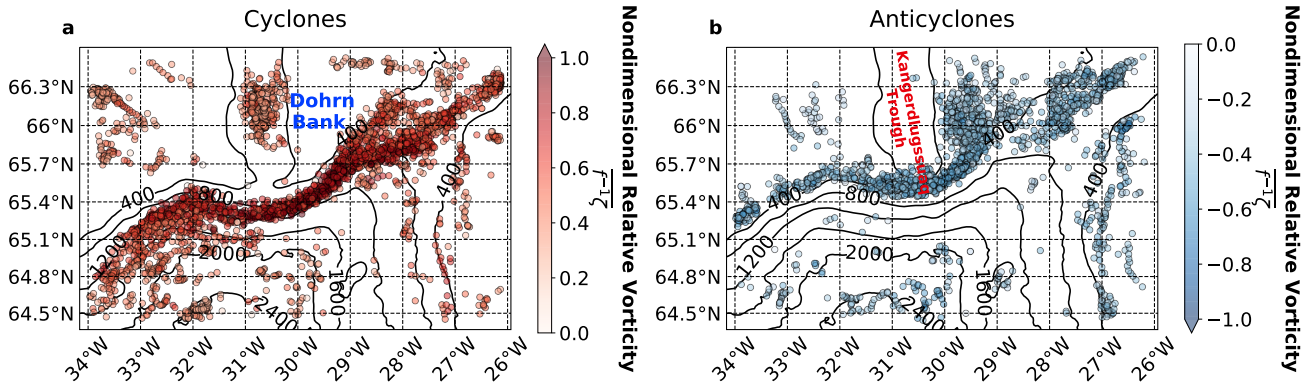

Figure S1. Unfiltered locations of the centers of the detected cyclones (a) and anticyclones (b). The color code indicates the mean nondimensional relative vorticity ($\overline{f^{-1}\zeta}$) of the vortices. ζ has been extracted along the σ-level at a depth of $5H/8$. Black contours show the seafloor depth in meters.